

Article

Chitosan-Biopolymer-Entrapped Activated Charcoal for Adsorption of Reactive Orange Dye from Aqueous Phase and CO₂ from Gaseous Phase

Pradip Nandanwar ¹, Ravin Jugade ^{1,*}, Vaishnavi Gomase ¹, Anita Shekhawat ¹, Apurva Bambal ¹, Dhandayutham Saravanan ² and Sadanand Pandey ^{3,*}

¹ Department of Chemistry, RTM Nagpur University, Nagpur 440033, India

² Department of Chemistry, National College, Tiruchirappalli 620001, India

³ Department of Chemistry, College of Natural Science, Yeungnam University, 280 Daehak-Ro, 38541 Gyeongsan, Gyeongsangbuk, Republic of Korea

* Correspondence: ravinj2001@yahoo.co.in (R.J.); sadanand.au@gmail.com or spandey@ynu.ac.kr (S.P.)

Abstract: Polymers have been proven to be an interesting class of adsorbents applied in water treatment. Biopolymers are of special interest due to their unique properties such as biocompatibility, biodegradability, and reusability. This work reports a composite formed by a chitosan biopolymer and activated charcoal using sodium citrate as a crosslinking agent. The chitosan–citrate-activated charcoal composite (CCA) was characterized using FT–IR, SEM, EDAX, XRD, TGA–DTA and BET surface area analysis. The material was found to be microporous in nature with a surface area of 165.83 m²/g that led to high adsorption capacities toward both the targeted pollutants. In an aqueous phase, the dye adsorption studies were carried out with reactive orange 16 (R-16) dye, while in a gaseous phase, CO₂ adsorption capacity was evaluated. Under optimum solution conditions, maximum R-16 dye removal capacity was found to be 34.62 mg g^{−1}, while in the gas phase the CO₂ adsorption capacity was found to be 13.15 cm³g^{−1}. Intrinsic microporosity of CCA resulted in an enhanced capture capacity for R-16 dye and carbon dioxide in the respective phases. Material sustainability studies were carried out to evaluate various sustainability parameters.

Keywords: sodium-citrate-crosslinked chitosan; reactive orange dye; water treatment; CO₂ sequestration; adsorption efficiency; sustainability studies



Citation: Nandanwar, P.; Jugade, R.; Gomase, V.; Shekhawat, A.; Bambal, A.; Saravanan, D.; Pandey, S. Chitosan-Biopolymer-Entrapped Activated Charcoal for Adsorption of Reactive Orange Dye from Aqueous Phase and CO₂ from Gaseous Phase. *J. Compos. Sci.* **2023**, *7*, 103. <https://doi.org/10.3390/jcs7030103>

Academic Editor: Francesco Tornabene

Received: 11 January 2023

Revised: 3 February 2023

Accepted: 28 February 2023

Published: 7 March 2023



Copyright: © 2023 by the authors. Licensee MDPI, Basel, Switzerland. This article is an open access article distributed under the terms and conditions of the Creative Commons Attribution (CC BY) license (<https://creativecommons.org/licenses/by/4.0/>).

1. Introduction

Natural polymers based on plant and non-plants sources have been in focus as adsorbents for the majority of contaminants in order to provide a clean and safe environment. Natural polymers cleanse wastewater for its sustainable recirculation into the environment due to their inherent structure, composition, and diverse functionality along with important characteristic properties such as non-toxicity, low-cost, renewability, biodegradability, and biocompatibility [1]. A variety of natural polymers such as starch [2], pectin [3], chitin, chitosan [4], bacteria, algae, fungi [5], and ghatti gum [6] have been employed for decontamination of water. Nonetheless, in many cases, natural polymers are not sufficient to remove the dyes from highly complex dye-containing wastewater, and so these polymers should be subjected to a modification process, involving chemical or physical treatment, in order to enhance their efficiency in removing dyes from complex wastewater [7]. Composites of biopolymers have dominant properties such as improved durability, processing capability, high functionality, and a large surface area, which increase the removal of contaminants or pollutants from the environment via adsorption [8]. Recently, composites of natural polymers have come into focus as adsorbents for the majority of contaminants. These natural polymers include cellulose [9], chitosan [10], sodium alginate [11], and other natural products [12] due to their abundance, non-toxicity, biodegradability, low cost, etc.

Chitosan is widely used as an adsorbent for contaminant removal in wastewater due to its distinct advantages of non-toxicity, cost-effectiveness, biodegradability, and super-high adsorption capacity [13]. However, due to its high solubility and swelling index in acidic media, and low surface area and mechanical strength, chitosan, on its own, is not a successful material for water treatment technology. Therefore, chemical modification through composition and/or a crosslinking process is an alternative way to increase mechanical resistance, reduce hydrophobicity and stabilize chitosan in acidic environments. A lot of research has been conducted on dye adsorption using chitosan in its native form [10] and on chitosan combinations such as chitosan/carbon composites [14], chitosan–vanadate films [15], cellulose/chitosan composites [16], surface-modified chitosan [17], chitosan-based cryogels [18], and β -cyclodextrin–chitosan-based cross-linked adsorbents [19]. Blending of chitosan with other organic moieties and introducing magnetic properties to the composites have resulted in high selectivity and adsorption efficiency towards target pollutants [20]. Advanced applications of natural-fiber-reinforced chitosan, chitosan blends and their nanocomposites have also been reviewed in the recent literature [21].

Equally, continuous emission of carbon dioxide, owed to anthropogenic activities, is the prime cause of damaging the ozone layer leading to global warming and to critical environmental concerns [22] along with serious human health hazards [23]. With an ambitious objective of reducing CO₂ emission, the Paris Agreement has been emerged as an international climate protocol [24]. For this reason, carbon capture arose as a prominent strategy aiming towards the reduction in emission of CO₂. Various technologies for carbon dioxide capture that have been employed include absorption [25], cryogenics [26], cycles of carbonation–calcination [27], the use of membranes [28], and adsorption [29]. Among all CO₂ removal technologies, adsorption technologies have shown great potential because of their reversibility and versatility [30]. Many biopolymer-based adsorbents have been developed for this purpose. Materials such as nanocrystalline cellulose-based composites [31], chitosan-based composites [32], aerocellulose-derived activated carbon monoliths [33], microcrystalline cellulose-based composites [34], nanofibrillated cellulose–polyethylenimine foams [35], chitin acetate/DMSO binary systems [36], chitosan-derived activated carbons [37], and chitosan–polybenzoxazine nanocomposites [38] have been used as adsorbents. The acidic character of the CO₂ molecule led to the development of basic solid sorbents through physical impregnation as well as chemical grafting of an amine compound onto a solid surface [39]. Chitosan, a biopolymer with an amino functionality, has been utilized as precursor for the synthesis of adsorbents for CO₂ capture [40]. Chitosan is obtained from the N-deacetylation of chitin, one of the most abundant polymers in the nature, which may be extracted from the carapace and exoskeleton of crustaceans [41]. The presence of free amino groups in the structure of chitosan can provide basic sites for the adsorption of CO₂, similar to other amino-based adsorbents.

Our research group has reported various chitosan- and cellulose-based materials for the removal of organic dyes from water bodies. These include a chitosan–alginate composite [42], a tetrabutyl ammonium impregnated chitosan [43], a chitosan–bentonite composite [44], a chitosan–Mohr’s salt composite [45], and a cellulose–tin composite [46]. Furthermore, recently, we have reported an ice-templated imidazole polymeric material for capture of CO₂ [47].

The aim of this work is to synthesize an environmentally benign material that can be used as a water-treatment agent as well as improve air quality without using any drastic conditions and chemicals. To the best of our knowledge, this work is the first ever attempt to derive a material at room temperature that has all the following merits: the adsorption properties of charcoal, the biocompatibility of chitosan, and mechanical stability provided by a citrate crosslinker. R-16 has been selected as a representative dye for this work. Such a material can be a boon to environmental scientists for multi-toxicant decontamination.

2. Materials and Methods

All the chemicals and reagents used were of analytical grade. Chitosan with a degree of deacetylation of >90% was purchased from Sisco Research Laboratory, Mumbai, India. Acetic acid and 25% ammonia solution were obtained from SD Fine Chemicals Ltd., Mumbai, India. Activated charcoal, sodium citrate, and reactive orange 16 dye were acquired from Loba Chemie, Mumbai, India. All chemicals were used without further purification and deionized distilled water was used throughout the studies.

Chitosan solution was prepared by dissolving 5 g chitosan in 500 mL of 2% acetic acid with stirring for 60 min. After the complete dissolution of chitosan in acetic acid, 2.5 g activated charcoal was added in small instalments and the solution was kept on gentle stirring for 30 min. The resultant solution was dripped into a beaker containing 1000 mL of 6% ammonia solution with the help of a syringe, leading to the formation of spherical beads. The fresh beads were rinsed with distilled water several times for removal of all traces of ammonia. The beads were suspended in 250 mL of 1% sodium citrate solution and stirred slowly at 40 °C for 2 h for the crosslinking process. The resulting CCA beads were washed with distilled water several times and dried overnight in a hot air oven at 50 °C. The beads were crushed using a pestle and mortar and sieved with a 100 micron mesh before being used in the adsorption experiments.

In each experiment, 25 mL dye solution of a pre-decided concentration along with a known weight of CCA, was stirred on a magnetic stirrer for a pre-determined time. It was then filtered and the residual R-16 dye concentration was evaluated spectrophotometrically at 493 nm using a Shimadzu 1900 UV-visible spectrophotometer (Shimadzu, Kyoto, Japan) with matched quartz cuvettes. Triplicate observations were obtained and the mean values are reported. The equilibrium adsorption efficiency in mg g^{-1} can be calculated using following equation [48].

$$q_e = \frac{C_0 - C_e}{W} \times V$$

where C_0 and C_e are the initial and equilibrium concentration of R-16 in solution in mg L^{-1} , respectively, V is the solution volume in L, and W is the weight of CCA used in g.

Trial runs were performed to compare the adsorption efficiencies of unmodified and sequentially modified adsorbents for the reactive orange16 dye. For this, 50 mg L^{-1} dye solution was equilibrated for 60 min with 100 mg of unmodified chitosan, activated charcoal, sodium citrate crosslinked chitosan, and CCA composite in different flasks. The solution phase concentrations in each flask were determined after filtration and the adsorption efficiency was calculated for each of them.

To study the effect of temperature as part of the evaluation of the thermodynamic parameters, the temperature was varied from 298 to 333 K. The quantity of adsorption of R-16 on CCA was investigated at an R-16 concentration of 100 mg L^{-1} using a 25 mL volume and adsorbent dose of 100 mg.

In all the experiments, the original solutions as well as the treated solutions were filtered through Whatman no. 1 filter papers to overcome the effect of adsorption by filter paper.

X-ray diffraction (XRD) spectra were recorded on an Ultima IV diffractometer (Cu Ka radiation, 40 kV and 20 mA) from $2\theta = 2^\circ$ to 10° with a step size of 0.02° (Rigaku, Tokyo, Japan). The thermal stability of the synthesized material (CCA) was assessed in a DTG-60 simultaneous DTA/TG instrument (Shimadzu, Tokyo, Japan) in nitrogen medium. About 15 mg of the sample was loaded on a platinum pan with a heating rate of $20^\circ\text{C min}^{-1}$ up to 900°C under 100 mL min^{-1} of flowing N_2 . Fourier transform infrared (FTIR) spectra were obtained on a BrukerAlphaE, London, UK, spectrometer in the range $500\text{--}4000\text{ cm}^{-1}$ using KBr pellets. The textural properties of the adsorbent were assessed using a scanning electron microscope (SEM) model TESCAN VEGA 3 SBH. Energy dispersive spectroscopy (EDAX) analysis was performed for elemental composition using an X-ray analyzer Oxford INCA Energy 250 EDS system during SEM observations. The samples were degassed at 150°C for 2 h under vacuum and N_2 adsorption/desorption isotherms were acquired

at $-196\text{ }^{\circ}\text{C}$ on a Quantachrome Nova 2200e analyzer (Anton Paar, Graz, Austria). The surface area was calculated by considering the BET model, and the pore volume was obtained using the BJH method. pHPZC was performed using an Equiptronics EQ-615 pH meter, the absorbance of the dyes was recorded using an Equiptronics EQ-824, while an Equiptronics magnetic stirrer model EQ-770 was used for batch adsorption stirring (Equiptronics, Mumbai, India).

The CO_2 adsorption capacity of the CCA material was evaluated using a Quantachrome Nova 2200e analyzer. The sample was pre-treated at $150\text{ }^{\circ}\text{C}$ under vacuum, and CO_2 adsorption isotherms were obtained at $25\text{ }^{\circ}\text{C}$ with pressures up to 1 bar.

Linear regression analysis was used to determine the parameters of isotherms and kinetic models. Additionally, error analysis was carried out to ascertain the desired accuracy has been achieved.

$$\text{SSE (error sum of squares)} = \sum (q_{e/t}^{\text{exp}} - q_{e/t}^{\text{cal}})^2$$

where $q_{e/t}^{\text{exp}}$ and $q_{e/t}^{\text{cal}}$ are the experimental adsorption capacity at equilibrium or at any time ($q_{e/t}^{\text{exp}}$) and the calculated adsorption capacity at equilibrium or at any time ($q_{e/t}^{\text{cal}}$) from the models, respectively.

$$\text{AIC (Akaike information criterion)} = N \ln \text{SSE}/N + 2K$$

where, N is the number of data points and K is the number of parameters [49].

3. Results

3.1. Characterization of CCA

FT-IR spectra of native chitosan showed (Figure 1a) its characteristic vibrational peaks at 1021 cm^{-1} (C–O–C stretching), 1641 cm^{-1} (N–H stretching), 2864 cm^{-1} (C–H stretching), and 577 cm^{-1} (C–H bending) [50]. When CCA was formed, these bands shifted to higher wavenumbers while the spectrum was found to be highly complex (Figure 1b). In addition to that, the peak observed at 698 cm^{-1} is due the C–H bending and deformation frequencies of the cross-linker sodium citrate. The C=O stretching band was found to get intensified at 1692 cm^{-1} . This indicates cross-linking of sodium citrate with chitosan involving electrostatic interactions [51].

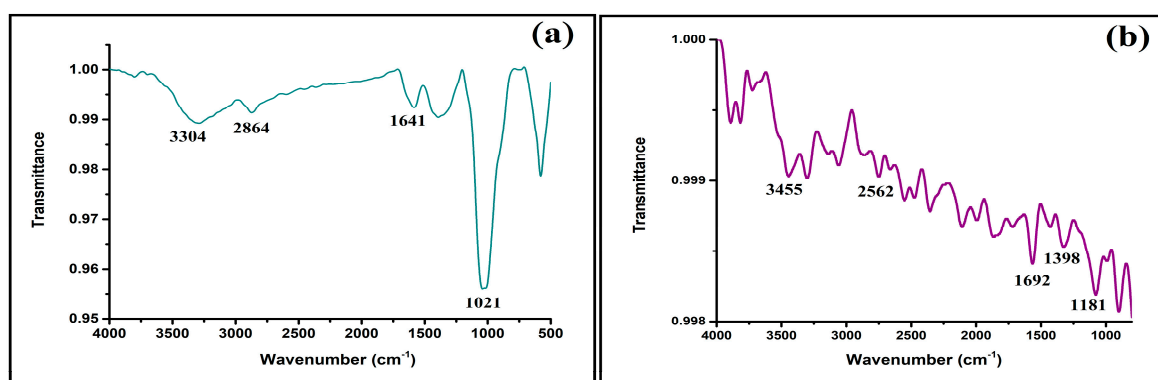


Figure 1. FTIR spectra of (a) chitosan and (b) CCA.

Figure 2 shows the X-ray diffractograms of chitosan and CCA. Native chitosan showed characteristic peaks at $2\theta = 10.92^{\circ}$ and 20.01° corresponding to (020) and (110) planes, respectively [52]. In case of CCA, these two peaks were found to shift towards lower values. The decrease in crystallinity of adsorbent can be attributed to the typical amorphous regions of chitosan which are established through intramolecular and intermolecular H-bonding interactions. The XRD pattern of CCA shows additional peaks at $2\theta = 44.56^{\circ}$, 72.7° , and 88.39° corresponding to various planes of sodium citrate [53].

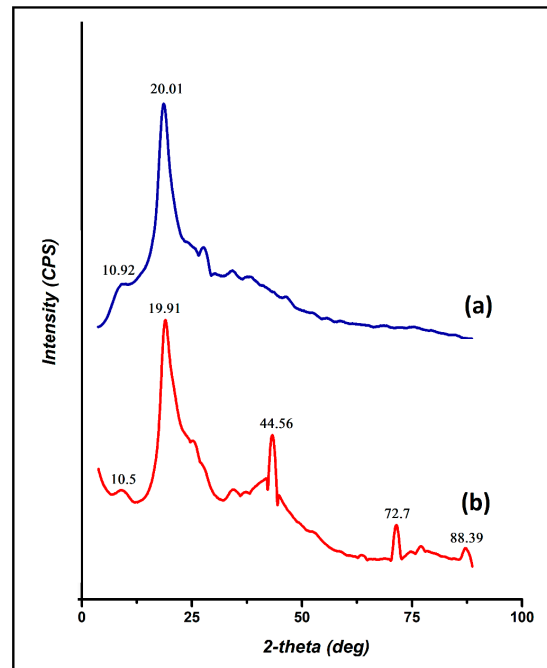


Figure 2. XRD patterns of (a) chitosan and (b) CCA.

Thermal analyses were performed to evaluate the stability of the adsorbent at elevated temperatures, as this property is important to ensure its further use during several temperature and pressure swings. The TGA curve (Figure 3a) of chitosan showed two sharp weight losses due to loss of moisture and adsorbed water up to 120 °C and thermal decomposition between 275 and 325 °C. The total weight loss was found to be almost 100%. The composite material CCA also exhibited two sharp weight loss events. The first started at ambient temperatures going up to approximately 150 °C and is associated with the loss of physically adsorbed water. The second loss occurred in the range 325–400 °C. This shows enhanced thermal stability in comparison to the native chitosan. A gradual decomposition occurred above 400 °C corresponding to the complete decomposition of chitosan and the destruction of citrate crosslinking. The DTA curves (Figure 3b) presented endothermic peaks corresponding to moisture loss in both the materials and exothermic peaks for thermal decay. The shift in exotherm to higher temperature in CCA is a clear indication of formation of composite between chitosan and activated charcoal with the citrate crosslinker, as well as increased thermal stability of CCA.

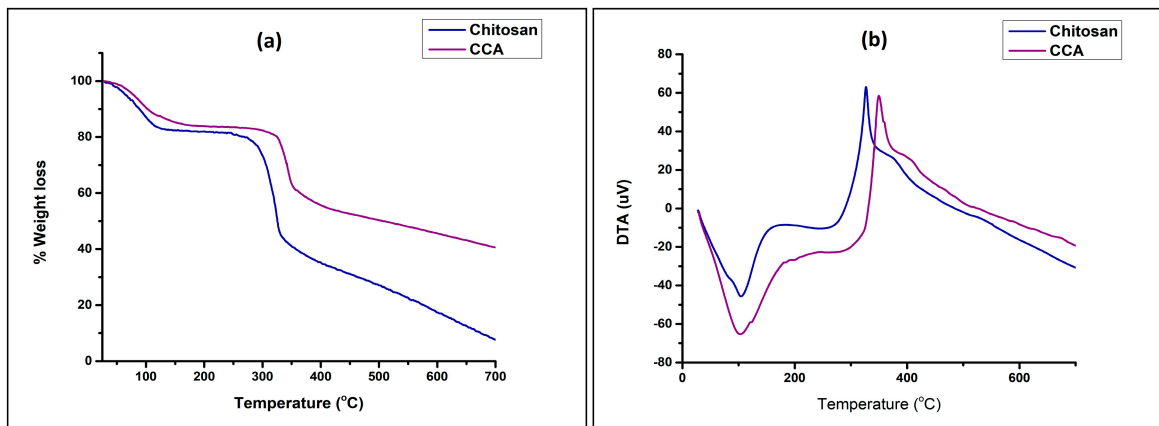


Figure 3. (a) TGA curves and (b) DTA curves of chitosan and CCA.

N_2 adsorption/desorption isotherms of CCA as depicted in Figure 4 showed the N_2 physisorption isotherm was type IV according to the IUPAC classification. This result indicated the presence of micropores in its structure. The pure chitosan was found to have a surface area of $0.013 \text{ m}^2 \text{ g}^{-1}$ with a pore volume of $1.263 \times 10^{-3} \text{ cm}^3 \text{ g}^{-1}$ while those of activated charcoal were $897.9 \text{ m}^2 \text{ g}^{-1}$ and $12.29 \text{ cm}^3 \text{ g}^{-1}$. This indicates a non-porous nature of chitosan and a highly porous nature of activated charcoal. The surface area of CCA was $165.83 \text{ m}^2 \text{ g}^{-1}$ with a pore volume of $1.332 \text{ cm}^3 \text{ g}^{-1}$. The mean pore radius of CCA was found to be 1.459 nm , indicating that it is a microporous material [54]. The intermediate surface area of CCA is indicative of formation of composite and loading of chitosan into the porous framework of activated charcoal. The adsorption–desorption isotherm shows a small hysteresis loop of the H4 type. Such a loop is observed if the material is highly complex showing microporosity as well as mesoporosity. This observation is consistent with the granular-like appearance of the surface of the material as obtained in SEM micrographs. The isotherm shows that desorption curves shifted to lower values than adsorption curves, which can be attributed to cavitation-persuaded desertion [55]. The high adsorption capacity of CCA towards R-16 dye can be prominently attributed to the high surface area, large pore volume, and micro and mesoporous nature of the adsorbent.

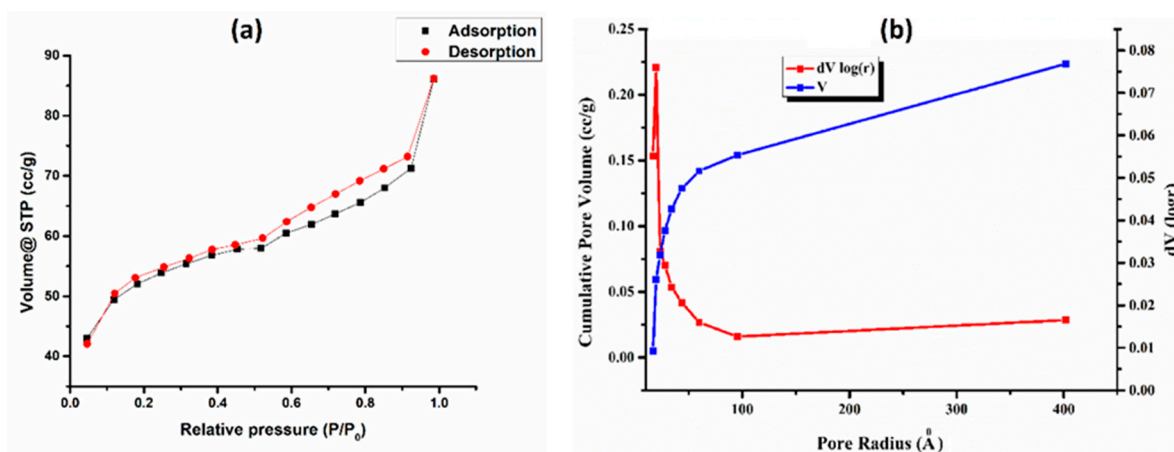


Figure 4. (a) N_2 adsorption–desorption isotherms; (b) pore size distribution of CCA.

The SEM micrographs show the surface morphology of the chitosan and the modified adsorbent (Figure 5). Chitosan has a relatively smooth and regular surface compared to CCA which has an irregular and heterogeneous surface. The porous and folded surface of the adsorbent enhances the surface area and therefore the adsorption capacity. The EDAX technique was used to analyze the elemental composition of CCA. Both chitosan and CCA have elemental C, N, and O as constituent elements, along with a slight impurity of Na in CCA.

3.2. Optimization of Adsorption Equilibrium Parameters

The pH of the R-16 dye solution greatly influences the adsorption process, and thus the impact of solution pH on adsorption was studied. The pH of the R-16 dye varied from pH 4.0 to 8.0 and was equilibrated with a 100 mg CCA dose for 60 min on magnetic stirrer. Figure 6a shows that the R-16 dye removal reached a maximum at pH 8. Under acidic conditions, the nitrogen atoms of both chitosan and R-16 dye get protonated, leading to repulsive interaction. Under stronger basic conditions, as the pH exceeds 8.2, the surface charge of CCA becomes negative and it repels the anionic dye molecules [56]. Hence, it is quite obvious that the electrostatic interaction is strongly attractive at a near-neutral pH between 7 and 8. Hence, pH 8.0 was maintained throughout the studies (Figure 6a). At pH 9.0, the surface charge of material becomes negative, thereby repelling the anionic dye. This could be reflected in a sudden decrease in adsorption efficiency at pH 9.0.

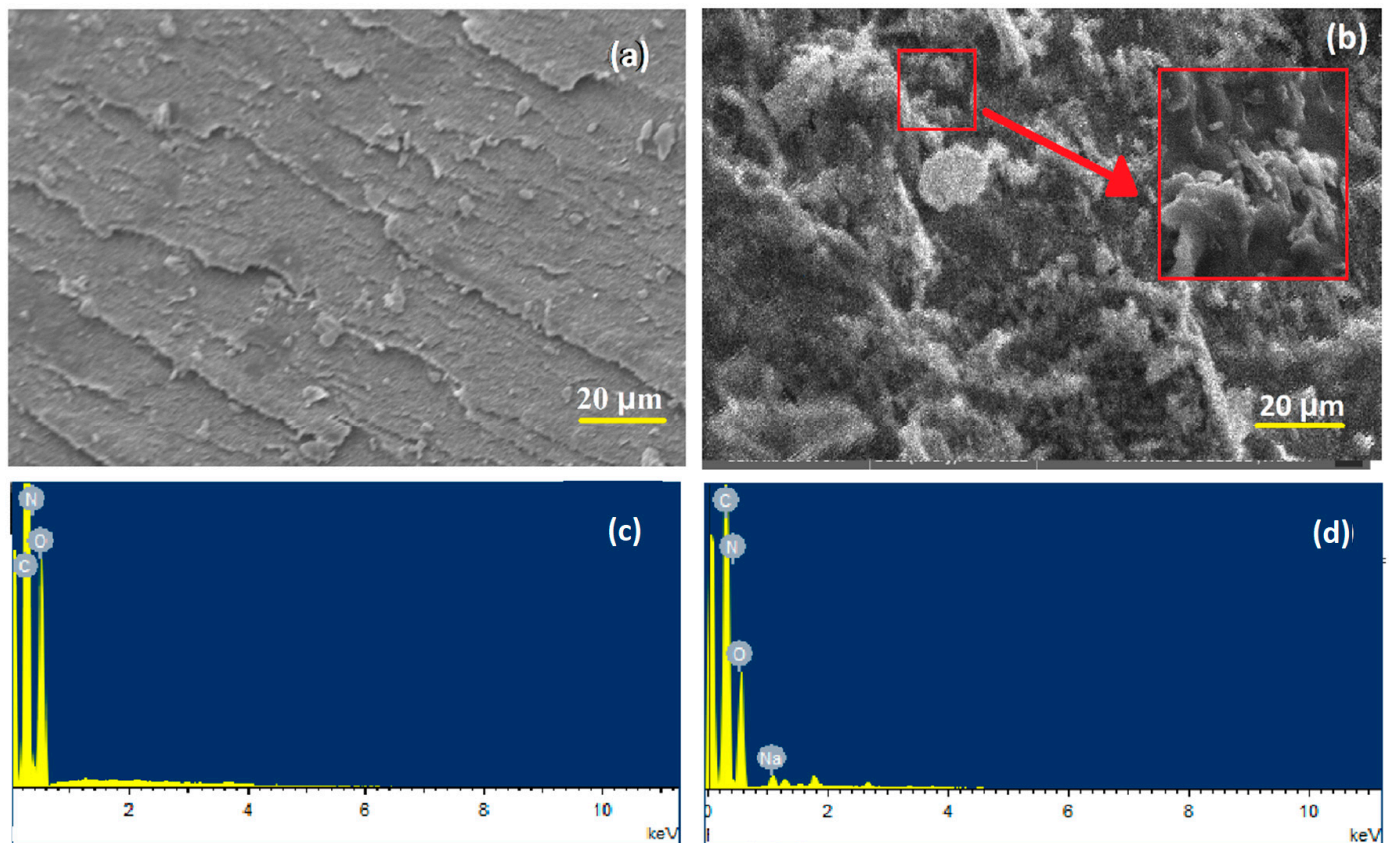


Figure 5. SEM micrographs of (a) chitosan and (b) CCA, and EDAX spectra of (c) chitosan and (d) CCA.

In order to determine the effect of CCA dosage on the removal of R-16 dye, the dose was varied from 25 mg to 300 mg and equilibrated with 100 mg L^{-1} R-16 dye for 60 min. With an increase in the adsorbent dose, the rate of adsorption was found to increase due to availability of more and more adsorption sites. When the available dye molecules were completely adsorbed, a plateau was obtained at above 100 mg adsorbent. The adsorption efficiency in terms of q_e (mg g^{-1}) was found to be high at lower adsorbent doses and further decreased with an increase in dose (Figure 6b). Above 100 mg adsorbent dose the removal of R-16 dye is more than 90% and thus 100 mg dose was fixed for further studies.

In order to determine the effect of contact time, the time was varied from 5 to 150 min. From Figure 6c, it can be seen that there is a rapid increase in adsorption up to 60 min, leading to saturation of adsorbent surface. Equilibrium was achieved, and so negligible variation was observed after this. Thus, 60 min time was fixed for further studies.

A range of initial R-16 dye concentrations were used in the adsorption studies, ranging from 25 mg L^{-1} to 500 mg L^{-1} . The study was carried out at previously optimized parameters with a fixed dose, time, and original pH of dye solution. More than 90% adsorption was observed up to 100 mg L^{-1} , then it decreased rapidly with further increase in dye concentration due to saturation of adsorbent surface (Figure 6d). The efficiency of material was found to be maximum at an R-16 dye concentration of 300 mg L^{-1} .

The surface charge on the adsorbent was evaluated using pH_{PZC} . It is the pH at which the charge on the adsorbent surface is zero. In order to determine pH_{PZC} , 50 mL of 0.1 M NaCl solutions which varied in pH from 2.0 to 9.0 were taken in separate conical flasks. 100 mg CCA was added to each system and the solutions were stirred for 24 h. The solutions were filtered, and the pH values of the filtrates were determined. From the plot of ΔpH versus initial pH, the pH_{PZC} of the adsorbent was determined to be 8.2 (Figure 7). When the solution pH is less than 8.2, the charge on the adsorbent surface is positive and

thus it will take up negative ions and when the charge on the adsorbent surface is negative it will take up positive ions [57].

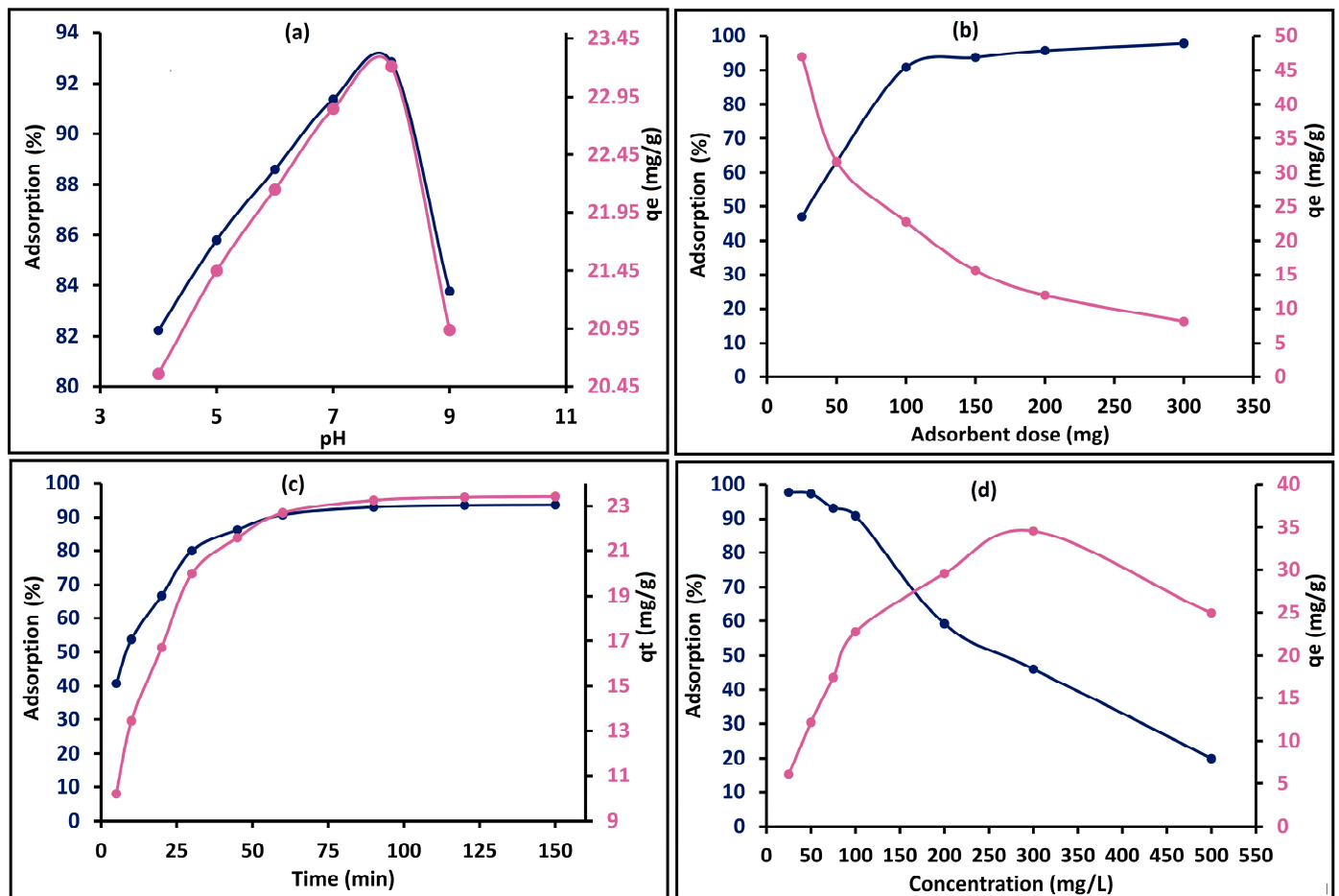


Figure 6. (a) Effect of pH, (b) effect of adsorbent dose, (c) effect of adsorption time, and (d) effect of concentration on adsorption of R-16 dye (Blue = Adsorption % and Pink = q_e).

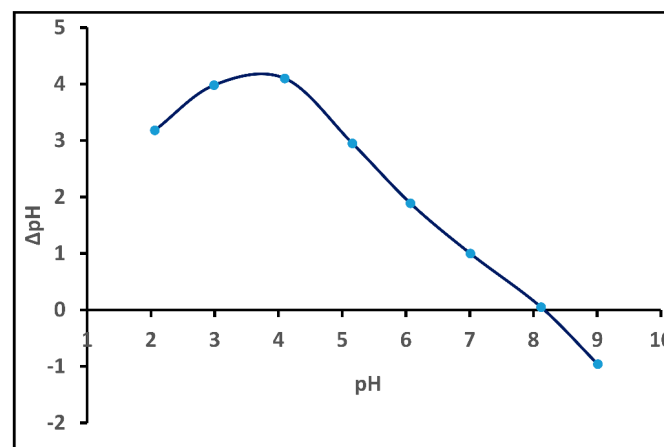


Figure 7. pH_{pzc} of CCA.

3.3. Screening Runs

In order to check the applicability of CCA for R-16 dye confiscation, the four materials were selected. A total of 100 mg each of chitosan, activated charcoal, citrate-crosslinked chitosan, and CCA was added to 25 mL of 100 mg L⁻¹ R-16 dye solution in separate conical

flasks and stirred for 60 min. The solutions were filtered and residual concentrations of filtrates were evaluated. The adsorption capacities and percentage adsorption of the four materials are compared in Figure 8. It was observed that all the four materials have a tendency to adsorb R-16 dye. However, the capacity was maximum for CCA with more than 90% adsorption. Hence, it can be concluded that CCA is an admirable adsorbent for R-16 dye.

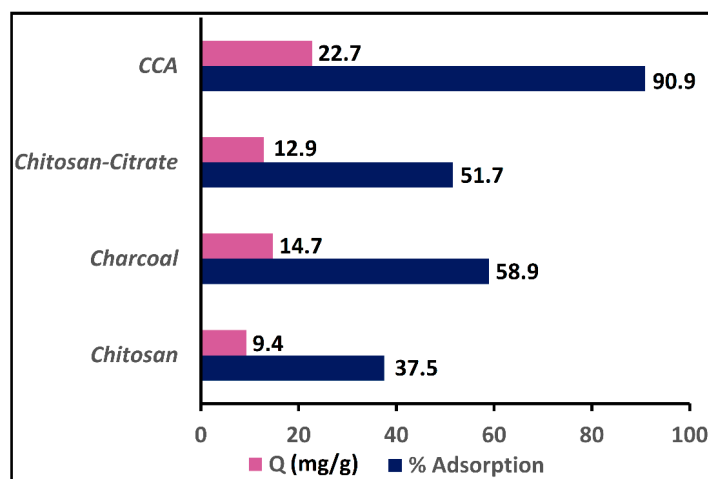


Figure 8. Comparison of various materials for removal of R-16 dye.

3.4. Isotherm Study

Adsorption isotherm models such as Freundlich [57] and Langmuir [58] were studied, which gave a better understanding of the adsorption mechanism (Figure 9a,b). The adsorption studies were carried by equilibrating 25 mL of R-16 dye solution by increasing the concentration from 25 to 500 mg L⁻¹ with 100 mg adsorbent for 60 min. From Table 1 it can be seen that the correlation coefficient value is quite close to unity for the Langmuir isotherm. From the R² value it can be concluded that there is a monolayer formation of R-16 on CCA in accordance with the Langmuir model. Additionally, the AIC value was found to be lower for the Langmuir model, indicating that it was the best fit model. The Freundlich isotherm shows the value of n is 3.67 which specifies a chemisorption process of adsorption. The adsorption capacity of R-16 dye is depicted in Table 1.

3.5. Kinetics of Adsorption

The measure of progress of R-16 dye adsorbed on the CCA depends on contact time and thus the kinetics of adsorption were studied using pseudo-first- and pseudo-second-order reactions. Experiments were carried out at concentration of 100 mg L⁻¹ by varying time from 5 to 150 min with 100 mg adsorbent. The plots of kinetics of adsorption for R-16 dye were studied and the results are depicted in Figure 9c,d. The values of the correlation coefficients for both models were found to be close to 1 and so an error analysis was carried out using AIC. As the value of AIC was lower for pseudo-second-order kinetics, it can be concluded that it is best model to describe the R-16 dye adsorption on CCA, affirming chemisorption. The results are summarized in Table 1. Additionally, an intraparticle diffusion model designed by Weber and Morris [59] was used to identify if the adsorption process is controlled by diffusion only. Figure 9e shows that the intercept between qt and t^{1/2} is non-zero, indicating that adsorption is a complex combination of both intraparticle diffusion and surface adsorption.

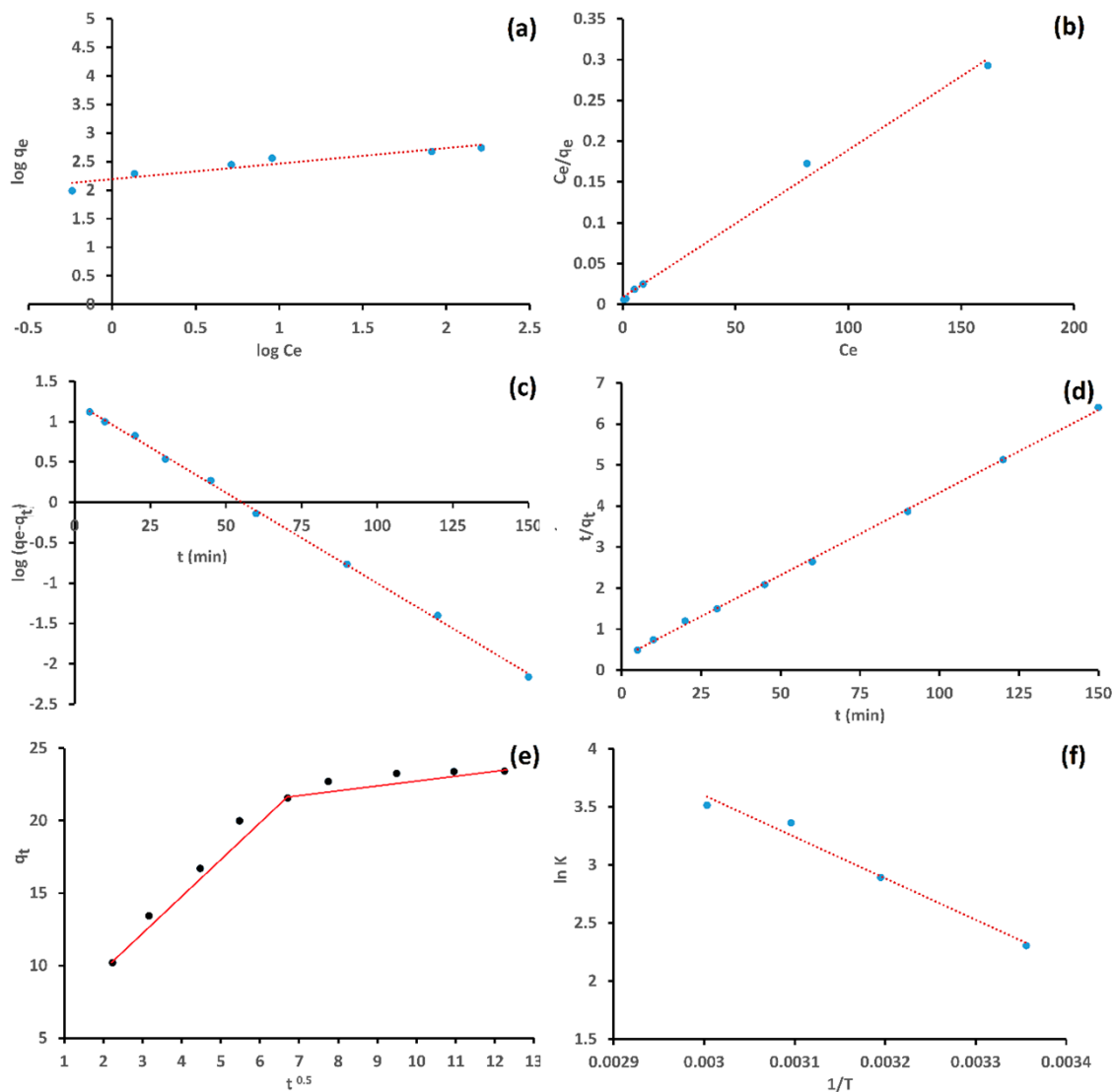


Figure 9. (a) Freundlich, (b) Langmuir, (c) Pseudo-first order (d) Pseudo-second order, and (e) intra-particle diffusion model. (f) van't Hoff plot.

3.6. Thermodynamics of Adsorption

The temperature has an influential effect on the adsorption process. The temperature effect was observed at temperatures 298 K, 313 K, 323 K, and 333 K. It was observed that the percent adsorption increases with an increase in temperature, indicating the chemisorption nature as a minimum amount of activation energy is required for the reaction to proceed. The values of Gibbs free energy (ΔG), enthalpy (ΔH), and entropy (ΔS) were obtained from intercept and slope of plot $\ln K$ versus $1/T$. The negative value of ΔG over the entire temperature range shows the process is spontaneous and exothermic. The positive values of ΔH and ΔS show that the process is entropy driven. The respective van't Hoff plots are shown in Figure 9f and the results are summarized in Table 2.

3.7. CO₂ Adsorption

Reported literature shows that native chitosan has a negligible CO₂ adsorption capacity [60]. Adsorption experiments were performed at 25 °C, within pressures up to 1 bar. Figure 10 shows the adsorption–desorption curve for CO₂ with an adsorption capacity of 13.15 cm³ g^{−1}. The composite materials showed higher adsorption capacities than the parent chitosan, but lower than the pure activated carbon supports. This later finding can be explained by the significantly higher BET area of the mesoporous activated carbons.

One may assume that CO₂ adsorption on the surface of the functionalized materials occurs through acid–base interactions with the amine groups of the chitosan polysaccharide chains. The accepted mechanism under anhydrous conditions takes place in two stages: First, there occurs a formation of a zwitterion intermediate through a nucleophilic attack of the amino group to the CO₂ molecule. Then, the zwitterion is deprotonated by another amine or basic site of the material to form a carbamate [61]. The increase in capture capacity in CCA from 2.24 cm³ g^{−1} for native chitosan by a factor of 5.87 times was an important outcome of this modification.

Table 1. Isotherm and kinetic parameters.

Adsorption Isotherm			
Sr. No.	Models	Parameter	Values
1	Langmuir	q _m (mg/g)	34.62
		b (L/mg)	0.0115
		R _L	0.634
		R ²	0.994
		AIC	41.15
2	Freundlich	K _F (mg ^{1−1/n} /g/L)	12.94
		n	3.671
		R ²	0.891
		AIC	57.26
Adsorption Kinetics			
1	Pseudo-first order	K ₁	0.050
		R ²	0.998
		AIC	261.30
2	Pseudo-second order	K ₂	0.004
		R ²	0.999
		AIC	65.30
3	Intraparticle diffusion	K _{int}	1.504
		R ²	0.847

Table 2. Thermodynamic parameters.

Temperature (K)	ΔG (kJ mol ^{−1})	ΔH (kJ mol ^{−1})	ΔS (J K ^{−1} mol ^{−1})
298	−5.711	29.699	119.01
313	−7.525		
323	−9.028		
333	−9.729		

3.8. Sustainability Parameters

The sustainability parameters indicate awareness towards environmental concerns during the formation of materials through chemical reactions. The raw materials used for synthesis were non-toxic. The sustainability parameters for CCA were analyzed in accordance with the reported literature [62] with respect to following parameters.

$$\text{Mass intensity} = \frac{\text{Mass of all materials used excluding water}}{\text{Mass of product}} \text{ kg kg}^{-1}$$

$$\text{Water intensity} = \frac{\text{Mass of all water used}}{\text{Mass of product}} \text{ kg kg}^{-1}$$

$$\text{Reaction mass efficiency} = \frac{\text{Mass of product}}{\text{Mass of all reactants}} \times 100$$

$$E - \text{factor} = \frac{\text{raw materials (kg)} - \text{desired product (kg)}}{\text{total product including water (kg)}}$$

All solutions were prepared in aqueous media. The mass intensity (Table 3) was found to be 2.97 kg kg⁻¹ which can be minimized avoiding the loss of product during filtration and washing. The values of water intensity and reaction mass efficiency need improvement in accordance with the reported literature. The low value of the E-factor shows the synthesis is environmentally friendly.

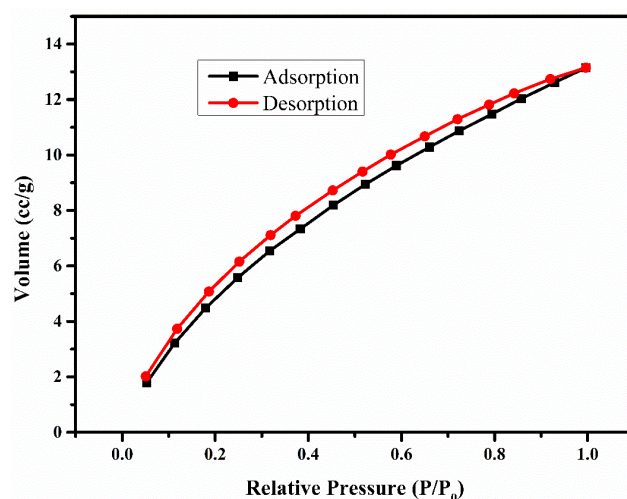


Figure 10. CO₂ adsorption–desorption curve of CCA at room temperature.

Table 3. Sustainability parameters.

Parameter	Values
Mass intensity	2.97 kg kg ⁻¹
Water intensity	2.28 kg kg ⁻¹
Reaction mass efficiency	39.02%
E-factor	0.47

These sustainability parameters are indicators of the fact that about 60% of the raw material used in the process is wasted, thereby reducing the atom economy. Efforts will further be made to improve the reaction mass efficiency. Such a material can be compared with itself under different experimental conditions. It was observed that these are the best conditions obtained for achieving the desired adsorption efficiency for the target pollutants.

3.9. Comparison of Adsorption Capacity

Table 4 shows adsorption capacities of various materials reported for the adsorption of R-16 dye. The table is self-explanatory and shows a comparative account of adsorption capacity with natural materials reported in the literature.

Table 4. Comparison with the reported literature.

Material	Adsorption Capacity (mg g ⁻¹)	Reference
Ethylene diamine-modified rice husk	16	[63]
Organofunctionalized kenyaite	33	[64]
Humin immobilized on silica	19.45	[65]
Surfactant zeolites	12.6	[66]
CCA	34.62	This work

4. Conclusions

A CCA composite was successfully synthesized and characterized using various techniques. The data obtained from the characterizations confirmed the formation of a composite. SEM micrographs and EDAX techniques showed surface modifications as well as its composition. BET surface area measurement, performed using the nitrogen adsorption–desorption method, revealed a microporous nature of the adsorbent. CCA was employed to remove R-16 dye from an aqueous medium, along with carbon capture. The amount of dye adsorption was dependent on the adsorbent dosage, temperature, and contact time. The maximum quantity adsorbed on CCA, obtained using the Langmuir model, was 34.62 mg g^{-1} . The thermodynamic data suggested that the adsorption of R-16 dye on CCA was spontaneous and endothermic in nature and was entropy-driven. The adsorption mechanism of the R-16 dye on CCA surface could be assigned to various types of interactions, such as electrostatic attraction or H-bonding interaction, while that of CO_2 on CCA could be due to Lewis acid–base interactions. The adsorption results indicated that CCA can be a promising alternative for the cleansing of aqueous as well as atmospheric environments from anionic dyes and CO_2 , respectively. Sustainability parameter evaluation has added a new dimension to the studies. The only area where further modification is required for this material is the reduction in porosity as compared to activated charcoal, thereby decreasing the CO_2 adsorption capacity.

Author Contributions: P.N.—methodology, writing first draft; R.J.—conceptualization, writing; review and editing, supervision; V.G.—data analysis, investigation, validation; A.S.—formal analysis; A.B.—data curation; D.S.—resources, S.P.—Writing, review and editing, supervision, funding. All authors have read and agreed to the published version of the manuscript.

Funding: This research received no external funding.

Data Availability Statement: Data will be made available on request.

Acknowledgments: The authors are grateful to RTM Nagpur University for instrumentation and laboratory facilities. Thanks to DST, New Delhi for DST-FIST grant and UGC for UGC-SAP support.

Conflicts of Interest: The authors declare no conflict of interest.

References

1. Kahu, S.; Shekhawat, A.; Saravanan, D.; Jugade, R. Ionic solid-impregnated sulphate-crosslinked chitosan for effective adsorption of hexavalent chromium from effluents. *Int. J. Environ. Sci. Technol.* **2016**, *13*, 2269–2282. [[CrossRef](#)]
2. Diana, S.; Orietta, L.; Alexandra, M.; Marta, F. Succiny lated Starches for Dye Removal. *Starch* **2021**, *73*, 2000043. [[CrossRef](#)]
3. Rakhshae, R.; Panahandeh, M. Stabilization of a magnetic nano-adsorbent by extracted pectin to remove methylene blue from aqueous solution: A comparative studying between two kinds of cross-liked pectin. *J. Hazard. Mater.* **2011**, *189*, 158–166. [[CrossRef](#)]
4. Samoila, P.; Enache, A.; Maria, C.; Harabagiu, V. *Chitin and Chitosan for Water Purification*; Wiley: Hoboken, NJ, USA, 2019. [[CrossRef](#)]
5. Das, M.; Adholeya, A. Potential Uses of immobilized bacteria, fungi, algae, and their aggregates for treatment of organic and inorganic pollutants in wastewater. *Water Chall. Solut. Glob. Scale* **2015**, *1206*, 319–337. [[CrossRef](#)]
6. Makhado, E.; Motshabi, B.; Allouss, D.; Ramohlola, K.; Modibane, K.; Hato, M.; Jugade, R.; Shaik, F.; Pandey, S. Development of a ghatti gum/poly (acrylic acid)/ TiO_2 hydrogel nanocomposite for malachite green adsorption from aqueous media: Statistical optimization using response surface methodology. *Chemosphere* **2022**, *306*, 35524. [[CrossRef](#)] [[PubMed](#)]
7. Jiang, X.; Li, Y.; Tang, X. Biopolymer-based flocculants: A review of recent technologies. *Environ. Sci. Pollut. Res.* **2021**, *28*, 46934–46963. [[CrossRef](#)] [[PubMed](#)]
8. Udayakumar, G.; Muthusamy, S.; Selvaganesh, B.; Sivarajasekar, N.; Rambabu, K.; Sivamani, S.; Sivakumar, N.; Maran, J.; Bandegharaei, A. Ecofriendly biopolymers and composites: Preparation and their applications in water-treatment. *Biotechnol. Adv.* **2021**, *52*, 107815. [[CrossRef](#)] [[PubMed](#)]
9. Abdelhamid, H.; Mathew, A. Cellulose-Based Materials for Water Remediation: Adsorption, Catalysis, and Antifouling. *Front. Chem. Eng.* **2021**, *3*, 790314. [[CrossRef](#)]
10. No, H.; Meyers, S. Application of chitosan for treatment of wastewaters. *Rev. Environ. Contam. Toxicol.* **2000**, *163*, 1–27. [[CrossRef](#)]

11. Bustos-Terrones, Y.; Bandala, E.; Moeller-Chávez, G.; Bustos-Terrones, V. Enhanced biological wastewater treatment using sodium alginate-immobilized microorganisms in a fluidized bed reactor. *Water Sci. Eng.* **2022**, *15*, 125–133. [[CrossRef](#)]
12. Pandey, S.; Kang, M. Modified biopolymer-locust bean gum based crosslinked hydrogels: Application in adsorption of cationic dye from aqueous solution. *Korean Soc. Ind. Chem.* **2019**, *1*, 155. Available online: <https://www.cheric.org/research/tech/proceedings/view.php?seq=181042> (accessed on 19 May 2019).
13. Saruchi, M.; Kumar, V.; Ghfar, A.; Pandey, S. A Green Approach for the Synthesis of Silver Nanoparticle-Embedded Chitosan Bionanocomposite as a Potential Device for the Sustained Release of the Itraconazole Drug and Its Antibacterial Characteristics. *Polymers* **2022**, *14*, 1911. [[CrossRef](#)]
14. Ahmed, M.; Hameed, B.; Hummadi, E. Review on recent progress in chitosan/chitin-carbonaceous material composites for the adsorption of water pollutants. *Carbohydr. Polym.* **2020**, *247*, 116690. [[CrossRef](#)] [[PubMed](#)]
15. Rodrigues, D.; Moura, J.; Dotto, G.; Cadaval, T.; Pinto, L. Preparation, Characterization and Dye Adsorption/Reuse of Chitosan-Vanadate Films. *J. Polym. Environ.* **2018**, *26*, 2917–2924. [[CrossRef](#)]
16. Wang, Y.; Wang, H.; Peng, H.; Wang, Z.; Wu, J.; Liu, Z. Dye Adsorption from Aqueous Solution by Cellulose/Chitosan Composite: Equilibrium, Kinetics, and Thermodynamics. *Fibers Polym.* **2018**, *19*, 340–349. [[CrossRef](#)]
17. Yildirim, A. Removal of the Anionic Dye Reactive Orange 16 by Chitosan/Tripolyphosphate/Mushroom. *Chem. Eng. Technol.* **2021**, *44*, 1371–1381. [[CrossRef](#)]
18. García-González, A.; Zavala-Arce, R.; Avila-Pérez, P.; Rangel-Vazquez, N.; Salazar-Rábago, J.; García-Rivas, J.; García-Gaitán, B. Experimental and theoretical study of dyes adsorption process on chitosan-based cryogel. *Int. J. Biol. Macromol.* **2021**, *169*, 75–84. [[CrossRef](#)] [[PubMed](#)]
19. Usman, M.; Ahmed, A.; Yu, B.; Wang, S.; Shen, Y.; Cong, H. Simultaneous adsorption of heavy metals and organic dyes by β -Cyclodextrin-Chitosan based cross-linked adsorbent. *Carbohydr. Polym.* **2021**, *255*, 117486. [[CrossRef](#)]
20. Eltaweil, A.; Hashem, O.; Abdel-Hamid, H.; El-Monaem, E.; Ayoup, M. Synthesis of a new magnetic Sulfacetamide-Ethylacetoacetate hydrazone-chitosan Schiff-base for Cr(VI) removal. *Int. J. Biol. Macromol.* **2022**, *222*, 1465–1475. [[CrossRef](#)]
21. Ilyas, R.A.; Aisyah, H.A.; Nordin, A.H.; Ngadi, N.; Zuhri, M.Y.M.; Asyraf, M.R.M.; Sapuan, S.M.; Zainudin, E.S.; Sharma, S.; Abral, H.; et al. Natural-Fiber-Reinforced Chitosan, Chitosan Blends and Their Nanocomposites for Various Advanced Applications. *Polymers* **2022**, *14*, 874. [[CrossRef](#)]
22. Gayathri, R.; Mahboob, S.; Govindarajan, M.; Al-Ghanim, K.; Ahmed, Z.; Al-Mulhm, N.; Vodovnik, M.; Vijayalakshmi, S. A review on biological carbon sequestration: A sustainable solution for a cleaner air environment, less pollution and lower health risks. *J. King Saud Univ.-Sci.* **2021**, *33*, 101282. [[CrossRef](#)]
23. Jacobson, T.; Kler, J.; Herrnke, M.; Braun, R.; Meyer, K.; Funk, W. Direct human health risks of increased atmospheric carbon dioxide. *Nat. Sustain.* **2019**, *2*, 691–701. [[CrossRef](#)]
24. Schleussner, C.; Rogelj, J.; Schaeffer, M.; Lissner, T.; Licker, R.; Fischer, E.; Knutti, R.; Levermann, A.; Frieler, K.; Hare, W. Science and policy characteristics of the Paris Agreement temperature goal. *Nat. Clim. Chang.* **2016**, *6*, 827–835. [[CrossRef](#)]
25. Rahmatmand, B.; Keshavarz, P.; Ayatollahi, S. Study of Absorption Enhancement of CO₂ by SiO₂, Al₂O₃, CNT, and Fe₃O₄ Nanoparticles in Water and Amine Solutions. *J. Chem. Eng. Data* **2016**, *61*, 1378–1387. [[CrossRef](#)]
26. Sateesh, C.; Nandakishora, Y.; Sahoo, R.; Murugan, S. Study of cryogenic CO₂ capture with solar-assisted VAR system. *Clean. Eng. Technol.* **2021**, *5*, 100351. [[CrossRef](#)]
27. Criado, Y.; Arias, B.; Abanades, J. Effect of the Carbonation Temperature on the CO₂ Carrying Capacity of CaO. *Ind. Eng. Chem. Res.* **2018**, *57*, 12595–12599. [[CrossRef](#)]
28. Luis, P.; Van Gerwen, T.; Van der Bruggen, B. Recent developments in membrane-based technologies for CO₂ capture. *Prog. Energy Combust. Sci.* **2012**, *38*, 419–448. [[CrossRef](#)]
29. Oliveira, D.; Chagas, J.; Ade Lima, A.; Mota, C. CO₂ Capture over MCM-41 and SBA-15 Mesoporous Silicas Impregnated with Chitosan. *Ind. Eng. Chem. Res.* **2022**, *61*, 10522–10530. [[CrossRef](#)]
30. Riboldi, L.; Bolland, O. Recent developments in membrane-based technologies for CO₂ capture. *Energy Procedia* **2017**, *114*, 2390–2400. [[CrossRef](#)]
31. Dassanayake, R.; Gunathilake, C.; Dassanayake, A.; Abidi, N.; Jaroniec, M. Amidoxime-functionalized nanocrystalline cellulose-mesoporous silica composites for carbon dioxide sorption at ambient and elevated temperatures. *J. Mater. Chem. A* **2017**, *5*, 7462–7473. [[CrossRef](#)]
32. Gregor, S.; Ganin, A. Sustainable CO₂ adsorbents prepared by coating chitosan onto mesoporous silicas for large-scale carbon capture technology. *Energy Technol.* **2015**, *3*, 249–258. [[CrossRef](#)]
33. Dassanayake, R.; Gunathilake, C.; Jackson, T.; Jaroniec, M.; Abidi, N. Preparation and adsorption properties of aerocellulose-derived activated carbon monoliths. *Cellulose* **2016**, *23*, 1363–1374. [[CrossRef](#)]
34. Gunathilake, C.; Dassanayake, R.; Abidi, N.; Jaroniec, M. Amidoxime-functionalized microcrystalline cellulose-mesoporous silica composites for carbon dioxide sorption at elevated temperatures. *J. Mater. Chem. A* **2016**, *13*, 4808–4819. [[CrossRef](#)]
35. Sehaqui, H.; Gálvez, M.; Becatinni, V.; Ng, Y.; Steinfeld, A.; Zimmermann, T.; Tingaut, P. Fast and Reversible Direct CO₂ Capture from Air onto All-Polymer Nanofibrillated Cellulose—Polyethylenimine Foams. *Environ. Sci. Technol.* **2015**, *49*, 3167–3174. [[CrossRef](#)]

36. Eftaiha, A.; Alsoubania, F.; Khaleel, I.A.; Carsten, T.; Aseel, H.; Qaroush, A. An investigation of carbon dioxide capture by chitin acetate/DMSO binary system. *Carbohydr. Polym.* **2016**, *152*, 163–169. [CrossRef] [PubMed]
37. Fujiki, J.; Yogo, K. The increased CO₂ adsorption performance of chitosan-derived activated carbons with nitrogen-doping. *Chem. Commun.* **2016**, *52*, 186–189. [CrossRef]
38. Alhwaige, A.A.; Ishida, H.; Qutubuddin, S. Carbon aerogels with excellent CO₂ adsorption capacity synthesized from clay-reinforced biobased chitosan-polybenzoxazine nanocomposites. *ACS Sustain. Chem. Eng.* **2016**, *4*, 1286–1295. [CrossRef]
39. Hu, X.E.; Liu, L.; Luo, X.; Xiao, G.; Shiko, E.; Zhang, R.; Fan, X.; Zhou, Y.; Liu, Y.Z.; Zeng, Y. A review of N-functionalized solid adsorbents for post-combustion CO₂ capture. *Appl. Energy* **2020**, *260*, 114244. [CrossRef]
40. Wu, Q.; Zhang, G.; Gao, M.; Huang, L.; Li, L.; Liu, S.; Xie, C.; Zhang, Y.; Yu, S. N-doped porous carbon from different nitrogen sources for high-performance supercapacitors and CO₂ adsorption. *J. Alloys Compd.* **2019**, *786*, 826–838. [CrossRef]
41. Rinaudo, M. Chitin and chitosan: Properties and applications. *Prog. Polym. Sci.* **2006**, *31*, 603–632. [CrossRef]
42. Khapre, M.; Pandey, S.; Jugade, R. Glutaraldehyde-cross-linked chitosan–alginate composite for organic dyes removal from aqueous solutions. *Int. J. Biol. Macromol.* **2021**, *190*, 862–875. [CrossRef]
43. Khapre, M.; Jugade, R. Tetrabutylammonium Impregnated Chitosan for Adsorptive Removal of Harmful Carcinogenic Dyes from Water-Bodies. *Chem. Afr.* **2021**, *4*, 993–1005. [CrossRef]
44. Khapre, M.; Jugade, R. Hierarchical approach towards adsorptive removal of Alizarin Red S dye using native chitosan and its successively modified versions. *Water Sci. Technol.* **2020**, *82*, 715–731. [CrossRef]
45. Korde, S.; Deshmukh, S.; Tandekar, S.; Jugade, R. Implementation of response surface methodology in physico-adsorption of Indigo carmine dye using modified chitosan composite. *Carbohydr. Polym. Technol. Appl.* **2021**, *2*, 100081. [CrossRef]
46. Khapre, M.; Shekhawat, A.; Saravanan, D.; Pandey, S.; Jugade, R. Mesoporous Fe–Al-doped cellulose for the efficient removal of reactive dyes. *Mater. Adv.* **2022**, *3*, 3278–3285. [CrossRef]
47. Nandanwar, P.; Jugade, R. Ice-templated fabrication of porous imidazole based polymers for CO₂ adsorption. *Indian J. Chem. B* **2021**, *60*, 881–887. Available online: <http://nopr.niscpr.res.in/handle/123456789/57735> (accessed on 1 January 2023).
48. Tandekar, S.; Saravanan, D.; Korde, S.; Jugade, R. Gamma degraded chitosan-Fe (III) beads for defluoridation of water. *Mater. Today Proc.* **2020**, *29*, 726–732. [CrossRef]
49. Radjai, H.; Ferkous, Z.; Jebali, H.; Majdoub, R.; Bourzami, G.; Raffin, M.; Achour, A.; Gil, M. Adsorptive removal of cationic and anionic dyes on a novel mesoporous adsorbent prepared from diatomite and anionic cellulose nanofibrils: Experimental and theoretical investigations. *J. Mol. Liq.* **2022**, *361*, 119670. [CrossRef]
50. Jeyaseelan, C.; Chaudhary, N.; Jugade, R. Sulphate-crosslinked chitosan as an adsorbent for the removal of Congo red dye from aqueous solution. *Air Soil Water Res.* **2018**, *11*, 1178622118811680. [CrossRef]
51. Agu, A.; Benablo, P.; Mesias, V.; Penalzoza, D. Synthesis and characterization of a chitosan-based citric acid-crosslinked Encapsulant system. *J. Chil. Chem. Soc.* **2019**, *64*, 4610–4612. [CrossRef]
52. Gomase, V.; Jugade, R.; Doondani, P.; Saravanan, D.; Pandey, S. Sequential modifications of chitosan biopolymer for enhanced confiscation of Cr (VI). *Inorg. Chem. Comm.* **2022**, *145*, 110009. [CrossRef]
53. Chen, M.; Runge, T.; Wang, L.; Li, R.; Feng, J.; Shu, X.; Shi, Q. Hydrogen bonding impact on chitosan plasticization. *Carbohydr. Polym.* **2018**, *200*, 115–121. [CrossRef] [PubMed]
54. Sing, K.; Williams, R. Physisorption hysteresis loops and the characterization of nanoporous materials. *Adsorp. Sci. Technol.* **2004**, *22*, 773–782. [CrossRef]
55. Korde, S.; Tandekar, S.; Jugade, R. Novel mesoporous chitosan-zirconia-ferrosiferrous oxide as magnetic composite for defluoridation of water. *J. Environ. Chem. Eng.* **2020**, *8*, 104360. [CrossRef]
56. Doondani, P.; Jugade, R.; Gomase, V.; Shekhawat, A.; Bambal, A.; Pandey, S. Chitosan/Graphite/Polyvinyl Alcohol Magnetic Hydrogel Microspheres for Decontamination of Reactive Orange 16 Dye. *Water* **2022**, *14*, 3411. [CrossRef]
57. Freundlich, H. Over the adsorption in solution. *J. Phys. Chem.* **1906**, *57*, 385–471.
58. Langmuir, I. The adsorption of gases on plain surfaces of Glass, Mica and Platinum. *J. Am. Chem. Soc.* **1918**, *40*, 1361–1403. [CrossRef]
59. Weber, W.; Morris, J. Kinetics of adsorption on carbon from solution. *J. Sanit. Eng. Div. Am. Soc. Civil Eng.* **1963**, *89*, 3–60. [CrossRef]
60. Chagas, J.; Crispim, G.; Pinto, B.; Gil, R.; Mota, C. Synthesis, Characterization, and CO₂ Uptake of Adsorbents Prepared by Hydrothermal Carbonization of Chitosan. *ACS Omega* **2020**, *5*, 29520–29529. [CrossRef]
61. Pietrelli, L.; Francolini, I.; Piozzi, A. CO₂ adsorption on crab shell derived activated carbons: Contribution of micropores and nitrogen-containing groups. *Sep. Sci. Technol.* **2015**, *50*, 1101–1107. [CrossRef]
62. Egor, M.; Kumar, A.; Ahuja, T.; Mukherjee, S.; Chakraborty, A.; Sudhakar, C.; Srikrishnarka, P.; Bose, S.; Ravindran, S.; Pradeep, T. Cellulosic Ternary Nanocomposite for Affordable and Sustainable Fluoride Removal. *ACS Sustain. Chem. Eng.* **2021**, *9*, 12788–12799. [CrossRef]
63. Lee, C.K.; Ong, S.T.; Zainal, Z. Ethylenediamine modified rice hull as a sorbent for the removal of Basic Blue 3 and Reactive Orange 16. *Int. J. Environ. Pollut.* **2008**, *34*, 246–260. [CrossRef]
64. Royer, B.; Cardoso, N.; Lima, E.; Ruiz, V.; Macedo, T.; Airoidi, C. Organofunctionalized kenyaite for dye removal from aqueous solution. *J. Colloid Interface Sci.* **2009**, *336*, 398–405. [CrossRef]

65. Jesus, A.M.D.; Romão, L.P.C.; Araújo, B.R.; Costa, A.S.; Marques, J.J. Use of humin as an alternative material for adsorption/desorption of reactive dyes. *Desalination* **2011**, *274*, 13–21. [[CrossRef](#)]
66. Fungaro, D.A.; Borrely, S.I.; Carvalho, T.E. Surfactant modified zeolite from cyclone ash as adsorbent for removal of Reactive Orange 16 from aqueous solution. *Am. J. Environ. Prot.* **2013**, *1*, 1–9. [[CrossRef](#)]

Disclaimer/Publisher's Note: The statements, opinions and data contained in all publications are solely those of the individual author(s) and contributor(s) and not of MDPI and/or the editor(s). MDPI and/or the editor(s) disclaim responsibility for any injury to people or property resulting from any ideas, methods, instructions or products referred to in the content.